Ti and O *K* edges for titanium oxides by multiple scattering calculations: Comparison to XAS and EELS spectra

Z. Y. Wu
Institut des Matériaux de Nantes, CNRS UMR 110, Laboratoire de Chimie des Solides, 2 rue de la Houssinière, 44072 Nantes Cedex 03, France
and INFN, Laboratori Nazionali di Frascati, Post Office Box 13, 00044 Frascati, Italy

G. Ouvrard and P. Gressier
Institut des Matériaux de Nantes, CNRS UMR 110, Laboratoire de Chimie des Solides, 2 rue de la Houssinière, 44072 Nantes Cedex 03, France

C. R. Natoli
INFN, Laboratori Nazionali di Frascati, Post Office Box 13, 00044 Frascati, Italy
(Received 10 July 1996; revised manuscript received 15 November 1996)

Theoretical simulations and interpretations of x-ray-absorption near-edge data at the Ti and O *K* edges in titanium oxides, rutile, and anatase, have been performed in the framework of full multiple scattering theory and a tight-binding linear muffin-tin orbital band-structure method. Good agreement between experimental data and theoretical calculations is obtained, especially in the preedge region of the Ti *K*-edge spectrum which is interpreted in terms of mixing between the central Ti $4p$ and neighboring Ti $3d$ orbitals in octahedral coordination. It is concluded that the positions of these latter Ti atoms relative to the photoabsorber influence in a noticeable way the intensity, width, and position of the features in the preedge region, which mainly originate from dipole transitions. Previous work on the subject is reexamined in the light of the present findings. [S0163-1829(97)01215-0]

I. INTRODUCTION

Titanium oxides display very interesting chemical and electronic properties in the field of catalysis, geological science, and high-T_c superconductivity.[1–4] Several titanium compounds have been investigated experimentally and theoretically by x-ray-absorption spectroscopy (XAS) and electron-energy-loss spectroscopy.[5–14] The interpretation of Ti and O *K*-edges structures presents an interesting problem, especially in the so-called preedge region, and is still controversial. We summarize the experimental results from Ref. 7 in Fig. 1 where Ti *K*-edge x-ray-absorption near-edge structure (XANES) spectra in both rutile and anatase are shown in the left panel, and the right panel contains O *K*-edge experimental electron-energy-loss near-edge structure (ELNES) data. We also present in Fig. 2 the molecular orbital (MO) energy level diagram often used in previous work to interpret absorption data.

In previous band-structure calculations,[10,11,15] the two prepeaks labeled $A3$ and B in the Ti *K* XANES spectra have been assigned to the $1s$ transitions to the t_{2g} and e_g bands which do not contain solely titanium d character, due to the hybridization of Ti $3d$ and $4p$ orbitals on different sites in the conduction band region.[11] Features $A1$ and shoulders $C2$ and $C3$ on the higher energy part of raising edge have not been interpreted satisfactorily in these studies. Brydson *et al.*[7] and Ruiz-Lopez and Munoz-Paez[12] tried to simulate all experimental data using a multiple scattering (MS) approach with various potentials, but their computations fail to give the good energy separations, the correct relative intensities and all transition structures; moreover their interpretation was not completely satisfactory, as will be discussed in the following. Both band-structure and MS calculations showed that the contribution of quadrupole transitions to the preedge intensity is not significant (less than 0.5% of the dipole contribution).

On the other hand, Uozumi *et al.*[16] adopted a $Ti_{11}O_6$ cluster model [see Fig. 3(a)] with a total Hamiltonian including quadrupole transition, the $1s$ core hole-$3d$ electron interaction, and the on site electron repulsion on the central absorbing atom. With a reasonable choice of the set of parameters appearing in the Hamiltonian and calculating only about 6 eV of the preedge region, they obtained a good agreement with experimental data. These authors have argued that the feature $A1$ is essentially due to a quadrupolar transition to $3d$ states of t_{2g} symmetry on the central atom, which are energetically shifted down from their unperturbed position by the $1s$ core-hole potential in a kind of excitonic mechanism. However in their model not all the ingredients of the relevant band structure were taken into account, since the $4p$ Ti states were neglected.

Angle resolved experimental XANES studies at Ti *K* edge in TiO_2 (rutile)[17,18] showed that preedge structures are angular dependent. In particular, the first peak $A1$ contains a B_{2g} component of d orbital symmetry.

In order to shed light on the type of transition involved, we present a series of *ab initio* full multiple scattering calculations of the XANES spectra at the Ti and O *K* edges for rutile and anatase compounds by using different choices for the cluster size around the photoabsorbing atom. In this way

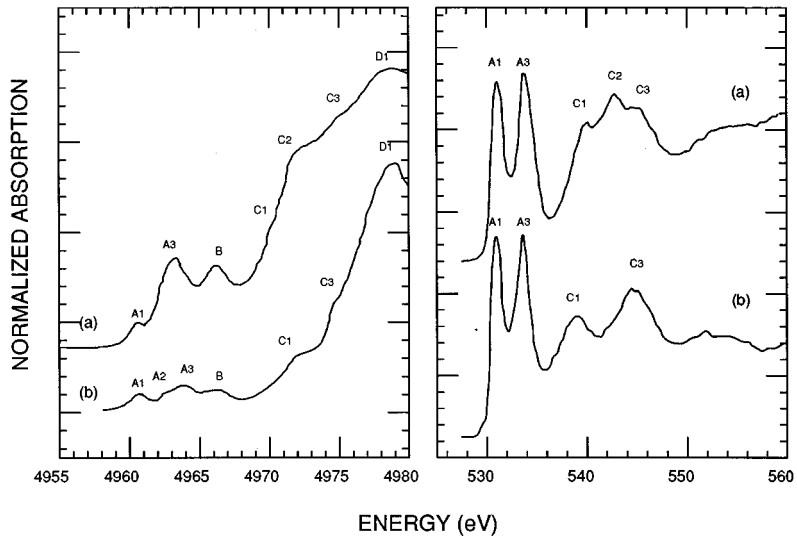

FIG. 1. The experimental curves obtained by Brydson *et al.* (Ref. 7). Left panel: Ti *K*-edge XANES spectra for rutile (a) and anatase (b); right panel: O *K*-edge ELNES spectra for rutile (a) and anatase (b). The peak positions are given in Table II.

we try to connect the specific atomic arrangement and the electronic structure of each titanium oxide with the position, sharpness, and intensity of the various features in the observed spectra. We also calculate the projected density of states derived on the basis of the tight-binding linear muffin-tin orbital (TB-LMTO) band-structure method. From a comparison between the different approaches, we try to reach some conclusions about the assignments of the various spectral features.

II. METHODS OF CALCULATION

All MS calculated XANES spectra are based on the one-electron MS theory[19–24] with XANES CONTINUUM code[25] which has been widely and successfully used to interpret the x-ray-absorption spectra in a variety of systems.[26] We use Mattheiss[27] prescription to construct the cluster density and obtain the Coulomb part of the potential by superposition of neutral atomic charge densities using Clementi and Roetti basis set tables.[28] For practical reasons we use the energy independent $X\alpha$ type of exchange followed by a Lorentzian convolution to account for inelastic losses of the photoelectron in the final state and the core hole width. The total width of the Lorentzian is given by $\Gamma_{\rm tot}(E)=2{\rm Im}\Sigma(E)+\Gamma_h$, where $\Sigma(E)$ is a volume averaged value of the Hedin-Lundqvist (HL) exchange and correlation potential (self-energy) $\Sigma(\vec{r},E)$ over the unit cell of the compound, as suggested by Penn.[29] We have chosen the muffin-tin radii according to the criterion of Norman,[30] and allowed a 10% overlap between contiguous spheres to simulate the atomic bond. The use of the $X\alpha$ exchange-correlation potential is not a limitation, since at low energies (around 30 eV above the onset of the absorption, the energy region we are interested in) this potential and the real part of the HL one roughly coincide if the constant α is appropriately chosen. In any case we have checked that for the biggest cluster calculations the two procedures (i.e., use of the $X-\alpha$ potential followed by Lorentzian convolution and use of the complex HL self-energy) give substantially identical results.

Density of states (DOS) calculations were performed using density-functional theory (DFT) within the local density approximation (LDA). For solving the one-electron Schrö-

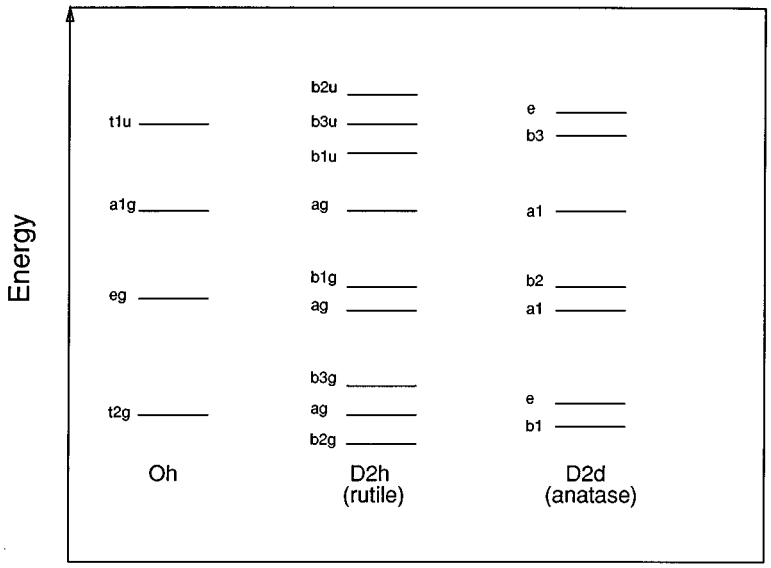

FIG. 2. Schematic energy levels diagram of the lowest unoccupied MO's of a $[TiO_6]^{8-}$ cluster with O_h, D_{2h} (rutile), and D_{2d} (anatase) symmetry.

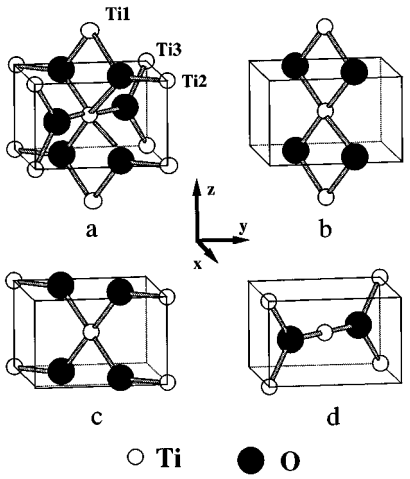

FIG. 3. (a) Tetragonal coordination structure of rutile. The small open sphere represents Ti and the big black one is oxygen. Connection between central Ti atom and surrounding Ti1 (b), Ti2 (c), and Ti3 (d) atoms is illustrated.

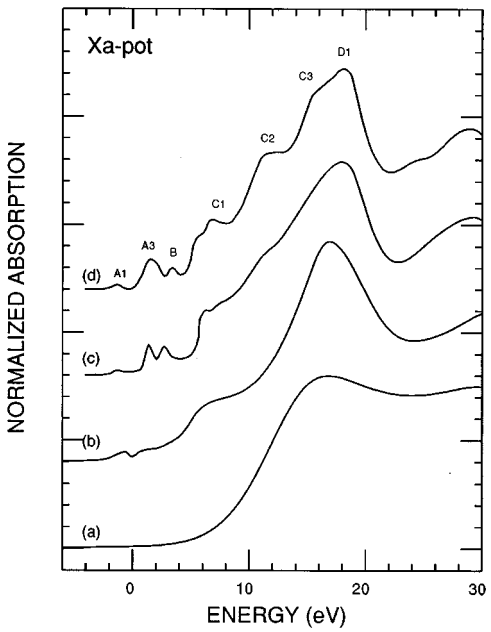

FIG. 4. Theoretical XANES spectra at the Ti K edge in the rutile compound as a function of cluster size by using the $X\alpha$ potential: (a) 7 atoms, (b) 25 atoms, (c) 51 atoms, and (d) 93 atoms.

dinger equation self-consistently we used the tight-binding representation of the scalar-relativistic linear muffin-tin orbital (LMTO) method in the atomic-spheres approximation (ASA) with the so-called combined correction.[31(a)] The usual LMTO-ASA criterion of totally filling the crystal volume by atomic spheres was used (i.e., the sum of all sphere volumes is equal to the unit cell volume). The Wigner-Seitz's atomic sphere radii have been determined by using the automatic procedure described in Ref. 31(b). In this procedure, the sphere radii are chosen under the requirement that the superposition of the spherical potentials be the best possible approximation to the full potential. The usual condition to get a high precision of the calculation is that the radial overlap of any couple of spheres is no more than 15% of the distance between the centers of the spheres, which is satisfied here by using empty site spheres. The atomic partial waves used in the calculations were $4s$, $4p$, and $3d$ for Ti atoms, $3s$, $2p$, and $3p$ for O atoms and $1s$ and $2p$ for the empty spheres. However, the $3s$ and $3p$ O states, and $2p$ empty-sphere states were not directly included in the basis set but ''down-folded'' using Löwdin's perturbation technique incorporated in the TB LMTO-ASA code.[31(c)] The k-space integrations were performed with the tetrahedron method.[31(d)] 1001 irreducible k points were included in the cycles towards self-consistency and 801 points were used to generate the densities of states.

LMTO-ASA calculations have been used for a long time on oxides, e.g., on $3d$ transition metals monooxides[31(a)] and more recently on high-T_c cuprates.[32(b)] Strictly speaking, DFT with local density approximation provides the eigenvalues of empty states which are not actual quasiparticles energies. However, one can be reasonably confident in DOS calculations just above the Fermi level,[33] as is the case in this study all the more that previous results obtained for TiS_2 and $LiTiS_2$ (Ref. 34) support this point of view. The reason for this is that the local density exchange-correlation potential in LDA calculations is nothing else that the HL self-energy calculated at or near the Fermi level for occupied states. Due to the slow variation of this latter for states lying in the energy range of about 10 eV above the Fermi level, one can be rather confident that the calculated DOS reflects the one calculated with the true HL potential. This conclusion is also born out by comparison with our cluster calculations, which yield similar DOS structures, as shown in the following. Of course the real problem in transition metal oxides is the introduction of electron correlations in the band calculation which nowadays is implemented via the LDA + Hubbard U approach.[35] However, being only interested in the gross features of the absorption spectra in rutile and anatase and in helping to resolve some controversial assignments, we have not felt that this was necessary.

III. RESULTS AND DISCUSSION

A. Ti K edge for rutile

Rutile has a tetragonal structure, the unit cell containing two titanium and four oxygen atoms [Fig. 3(a)], with lattice constants $a_0=4.594$ Å and $c_0=2.959$ Å.[36] The coordinating oxygen octahedron around the titanium atom is slightly distorted with two different bond lengths: two Ti-O distances at about 1.9803 Å and four others at 1.9487 Å. The point group symmetry with respect to the Ti site is D_{2h}. In Fig. 4 we report the theoretical calculations of Ti K-edge XANES spectra for rutile by using fully relaxed final state potential obtained within the $Z+1$ approximation[24] and four different cluster models (7, 25, 51, and 93 atoms) up to size convergence. The last one contains all atoms within 6 Å from the Ti photoabsorber taken as the center of the cluster.

For a Ti central atom, the first shell, including six oxygen, gives rise to a broad peak which corresponds to transition to Ti p-like final states. After adding the second shell made of Ti atoms, the prepeak $A1$ appears indicating that this feature reflects transitions to Ti $4p$ mixed with $3d$ orbitals of this higher Ti coordination shell. In order to illustrate its origin,

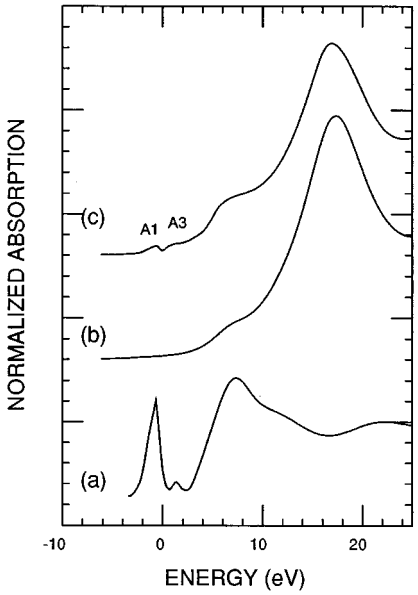

FIG. 5. MS calculations of the Ti *K*-edge XANES in rutile. (a) Simplified atomic cluster: central Ti plus ten surrounding Ti atoms (two at 2.959 Å and eight at 3.569 Å). (b) Simplified atomic cluster: central titanium plus 14 oxygen atoms (four at 1.948 Å, two at 1.980 Å, four at 3.487 Å, and four at 3.560 Å). (c) The same as curve (b) in Fig. 4.

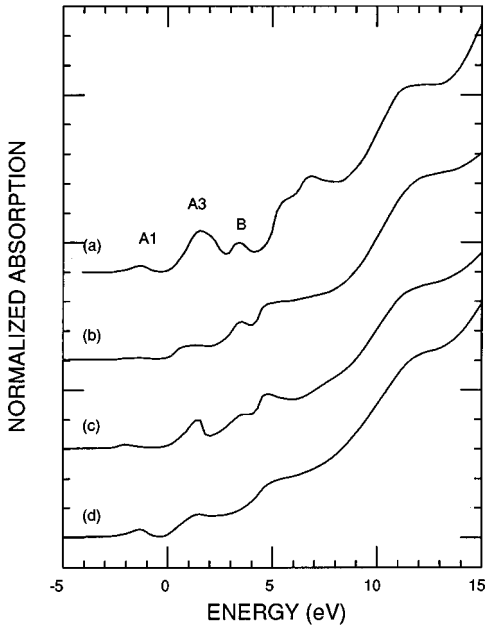

FIG. 6. MS calculations of the Ti *K*-edge XANES in rutile. (a) Normal 93-atom cluster as used in Fig. 4(d). (b) Simplified cluster calculation with the same size as used for (a) (93-atom cluster), but by taking into account solely two Ti1 at 2.959 Å in the second Ti shell (i.e., suppressing four Ti2 and four Ti3 at 3.569 Å as shown in Table I). (c) The same as (b) but only taking into account four Ti2 atoms (suppressing two Ti1 at 2.959 Å and four Ti3 at 3.569 Å). (d) The same as (c) but taking into account four Ti3 as shown in Table I (suppressing two Ti1 at 2.959 Å and four Ti2 at 3.569 Å from the cluster).

we present in Fig. 5 two calculations compared to the above 25-atom cluster result. A simplified 11 Ti atoms cluster, i.e., central Ti plus the already considered Ti shell, two Ti1 at 2.959 Å, four Ti2 and four Ti3 at 3.569 Å as tabulated in Table I and shown in Fig. 3, already gives rise to a sharp peak $A1$, whose intensity is due to direct Ti-Ti interaction, and a relatively weak $A3$ structure [curve (a)]. Similarly the intense feature at about 7 eV in curve (a) is due to a direct Ti-Ti interaction without the intervention of the surrounding oxygen ligands. On the contrary, a simplified 15 atoms cluster, central Ti plus 14 oxygen, does not show any feature in this region [curve (b)]. The lack of peak A in this latter calculation confirms that its presence is to be associated with the existence of unoccupied states made up of mixed Ti-4p orbitals with higher-shell Ti-3d orbitals. However full MS effects in the 25 atom cluster severely modify the intensity and the energy separation of the $A1$ and $A3$ components, giving rise to the absorption spectrum shown by curve (c), These findings point to the fact that the pre-edge A doublet is due to the interaction of the central Ti 4p orbitals with higher-neighbor Ti 3d orbitals, but also show that a 25 atom cluster is insufficient to reproduce the observed spectral features.

The spectral modification observed in passing from a 25- to 51-atom cluster is very striking and interesting: a new peak arises on the high energy side of the A doublet and at the same time the intensity and energy separation of the

TABLE I. Coordinates and interatomic distances (in Å) in a 4 Å radius cluster around a Ti photoabsorber. Only symmetrically nonequivalent atoms are included. The point groups are D_{2h} and D_{2d} for rutile and anatase, respectively. The z axis is along the c axis of the compounds.

	Atom	x	y	z	Dist.	Atom	x	y	z	Dist.
			TiO_2-rutile					TiO_2-anatase		
1	Ti×1	0.0000	0.0000	0.0000	0.0000	Ti×1	0.0000	0.0000	0.0000	0.0000
2	O×4	0.8968	−0.8968	1.4795	1.9487	O×4	1.3378	1.3378	0.3986	1.9335
3	O×2	1.4003	1.4003	0.0000	1.9803	O×2	0.0000	0.0000	1.9799	1.9799
4	Ti1×2	0.0000	0.0000	2.9590	2.9590	Ti1×4	1.3378	1.3378	2.3785	3.0392
5	O×4	1.4003	−3.1937	0.0000	3.4873	Ti2×4	2.6757	2.6757	0.0000	3.7840
6	O×4	1.4003	1.4003	2.9590	3.5605	O×8	0.0000	2.6757	2.7771	3.8564
7	Ti2×4	2.2970	2.2970	1.4795	3.5695					
8	Ti3×4	2.2970	−2.2970	1.4795	3.5695					

TABLE II. Qualitative assignments of all transition peaks in MS calculations and experimental Ti K-edge XANES and O K-edge ELNES spectra of TiO_2 polymorphs. ΔE_{exp} is from Ref. 7.

	Rutile			Anatase		
Peaks	ΔE_{MS} [a]	ΔE_{exp}	Assignments [b]	ΔE_{MS} [a]	ΔE_{exp}	Assignments [b]
			Ti K edge (eV)			
$A1$	-2.8	-3.1	b_{2g}, a_g, b_{3g} $(3d\text{-}4p)$	-2.8	-3.2	b_1, e $(3d\text{-}4p)$
$A2$				-1.36	-1.3	b_2, e $(3d\text{-}4p)$
$A3$	0.0	0.0	a_g, b_{1g} $(3d\text{-}4p)$	0.0	0.0	b_2, a_1 $(3d\text{-}4p)$
B	2.2	3.0	a_g $(4p\text{-}4s)$	2.6	2.3	a_1 $(4p\text{-}4s)$
$C1$	5.6	6.1	b_{1u} $(4p_z)$			
$C2$	9.5	8.6	b_{2u} $(4p_y)$	8.2	7.5	b_3 $(4p_z)$
$C3$	13.8	12.6	b_{3u} $(4p_x)$	11.0	11.1	e $(4p_x, 4p_y)$
$D1$	16.2	15.6	higher-lying np	17.2	15.9	higher-lying np
			O K edge (eV)			
$A1$	-2.35	-2.58	b_{2g}, a_g, b_{3g} $(3d\text{-}2p)$	-2.7	-2.58	$b_1, e(3d\text{-}2p)$
$A3$	0.0	0.0	a_g, b_{1g} $(3d\text{-}2p)$	0.0	0.0	b_2, a_1 $(3d\text{-}2p)$
$C1$	4.85	6.42	b_{1u} $(2p\text{-}4p)$			
$C2$	9.35	9.02	b_{2u} $(2p\text{-}4p)$	5.44	5.42	b_3 $(2p\text{-}4p)$
$C3$	12.15	11.42	b_{3u} $(2p\text{-}4p)$	11.8	10.92	e $(2p\text{-}4p)$

[a] ΔE is aligned by setting peak A_3 to zero on energy scale.
[b] The majority character of the conduction band states is given first.

components of the A doublet modify in such a way as to resemble more closely the experimental spectrum [Fig. 4(c)]. The reason for this is rather clear. One needs to take into account higher coordination neighbors (the next-nearest Ti shell plus surrounding oxygen atoms) in order to construct the appropriately hybridized t_{2g}-like and e_g-like molecular orbitals around each Ti atom in the cluster which are made up of $3d$ metal orbitals and $2p$ oxygen orbitals. The 51 atom cluster in fact already includes enough oxygen around Ti1, Ti2, and Ti3 to form octahedra whose orbitals mix with the $4p$ states of the central atom. Furthermore, these neighboring octahedra strongly interact with each other and cause molecular orbitals to overlap, forming extended energy bands and modifying their energy position. Figure 6 shows the 93-atom cluster calculation compared with calculations showing the scattering contributions from each of the three different titanium neighboring subshells (see Table I). The cluster size is identical in all cases and each time we just remove from the cluster the Ti atoms in the chosen subshell, e.g., in Fig. 6(b) we suppress four Ti2 and four Ti3. We can see that the two Ti1 at 2.95 Å [Fig. 6(b)] contribute to a broad peak $A3$; the four Ti2 at 3.5695 Å [Fig. 6(c)] contribute to a part of $A1$ as well as to $A3$; the four other Ti3 at the same distance but at different positions [Fig. 6(d)] also contribute to both peaks. All these three Ti subshells give different contributions to $A1$ and $A3$ peaks by the different ways of hybridization between their $3d$ octahedral orbitals and the central Ti $4p$ orbitals. The final result of the 93 atom cluster for the pre-edge region is approximately obtained by summing the individual scattering contributions from these ten Ti atoms. The average energy separation of the prepeaks $A1$ and $A3$ almost coincides with the crystal-field splitting of the t_{2g} and e_g orbitals (see below). All features observed in the experimental spectrum, especially in the preedge region, are reasonably well reproduced in the last large cluster calculation, not only in relative intensities but also in energy separations (see Table II). This points out that a 93-atom cluster is sufficient to describe bulk properties and that the prepeaks are, at the same time, very sensitive to the ''medium-range'' order of the solid. They might therefore be used to monitor such order.

In order to be able to identify the origin of the third peak in the preedge region and at the same time obtain a confirmation for the assignment of features $A1$ and $A3$, we present in Fig. 7 the calculated DOS just above the Fermi level E_f based on a TB-LMTO band-structure calculation, which has been widely used for this type of systems.[31] As is well known,[20] in MS calculations the absorption coefficient is proportional, through a smoothly varying radial matrix element, to the density of states, projected onto the photoabsorbing atom and relative to the angular momentum allowed by the dipole selection rule, of the cluster sampled by the excited photoelectron due to its limited mean-free path in the final state. The origin of the energy scale has been arbitrarily fixed at Fermi level E_f. There are three peaks in the Ti p-projected DOS corresponding to $A1$, $A3$, and B observed in the XANES spectrum and MS calculations. From the corresponding d-projected DOS one can easily conclude that features $A1$ and $A3$ are due to dipole transitions to Ti $4p$ states hybridized with crystal field split Ti $3d$ orbitals on neighboring Ti atoms, i.e., to t_{2g} and e_g-like band states. Peak B has mainly p character as shown by the Ti p-projected DOS so that it can be assigned to the transition to central atom $4p$ orbital hybridized with neighboring Ti $4s$ and/or O $2p$ a_g-type orbitals[10] as suggested by the orbital diagram sketched in Fig. 2. On the basis of the same diagram, one can assign features $C1$, $C2$, and $C3$ to Ti $4p$ states with b_{1u}, b_{2u}, b_{3u} character, respectively, hy-

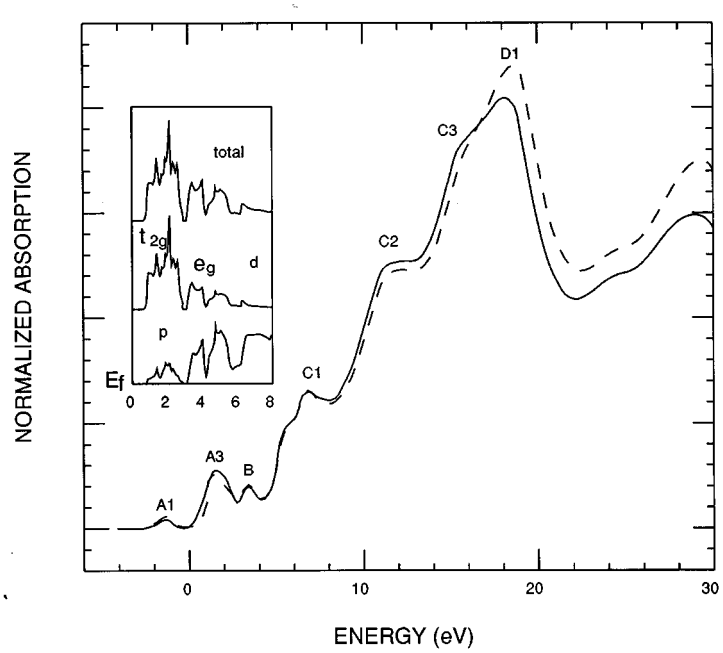

FIG. 7. The last model calculation as used in Fig. 4(d) (93-atom cluster) as a function of potential: full relaxed final state (solid line) and ground state (dash line) potential. The inset gives the theoretical TB-LMTO Ti p-DOS (lower curve) multiplied by 30, d-DOS (middle curve) and total unoccupied DOS (upper curve).

bridized with O $2p$ states of the same symmetry. Finally the main peak $D1$ is associated with electronic transitions to higher-lying p states.[7,11,12] The presence of peaks $C2$ and $C3$ in the one-electron MS calculations, which neglect many-electron effects, indicates that their assignment to $1s \rightarrow 4p$ shakedown transitions[10] seems unnecessary.

We present also ground state potential calculations, which ignore core-hole relaxation effects (dash line in Fig. 7) and which in the preedge region is almost identical with fully relaxed excited potential calculations. This finding is not surprising since the preedge features reflect the density of states associated with the medium-range order of the solid, as illustrated above, so that they should be rather insensitive to the details of the potential on the central Ti atom. All experimental peak positions in the Ti K-edge spectrum are tabulated in Table II and compared with those calculated on the basis of our MS calculations. They are all referred to peak $A3$ which therefore has been taken as the energy origin.

The present assignment for the preedge region is at a variance with that suggested in Refs. 15 and 16, where peaks $A3$ and B are associated with dipole transitions to t_{2g} and e_g-like band states, whereas peak $A1$ and a small component of peak $A3$ are assigned to a purely quadrupolar transition to $3d$ states on the central absorbing atom of the same symmetry (t_{2g} and e_g, respectively), shifted down in energy by the attractive core-hole potential in the final state.

Even though one cannot exclude *a priori* the presence of a quadrupolar transition in the preedge region (but our calculated intensity for it is less than 1% of the dipolar one), we are rather reluctant to accept this kind of assignment. The main motivation in Ref. 16 for invoking a kind of excitonic down shift for the quadrupolar transition was the presence of only two peaks in the calculated one-electron DOS. However we have shown that this is not the case, both in our full MS calculations (which reproduce other similar calculations[7,12]) and in the band-structure calculations.

More in detail, in Ref. 16 a Hubbard model has been considered for a $Ti_{11}O_6$ cluster with $3d$ states of the relevant symmetry on the Ti atoms and $2p$ states on the oxygen atoms. However $4p$ states, which have been shown to be important for the appearance of peak B, were not included. Moreover the cluster considered was not sufficient, as discussed above. Even considering the presence of the attractive potential in the final state due to the core hole, this by itself would not be sufficient to create the excitonic effect invoked in Ref. 16. One should in fact consider that in these compounds the back-bonding mechanism acts in such a way that the Ti atoms in the solid are almost neutral, possessing therefore nearly two electrons on average of partial $3d$ character. The Coulomb repulsion of the third excited electron might therefore compensate for the core-hole attraction. In the model used in Ref. 16, due to the separation of the dipolar and quadrupolar Hamiltonians, not enough $3d$ electrons on the central Ti atom were allowed. Therefore the intrasite repulsion was underestimated. It is very likely therefore that there is no down shift of the quadrupolar component. As a consequence we are led to believe that the experimentally observed quadrupolar transition falls nearly on top of the dipolar one, as experimentally seems indeed to be the case.[18] The only unexplained feature at the moment is the unexpectedly strong intensity of the quadrupolar transition which might be phonon assisted, as the dipolar one. A further confirmation for our present assignment of features $A1$, $A3$, and B will also come from the comparison with the O K-edge spectra.

B. Ti *K* edge for anatase

Anatase has a tetragonal structure containing twelve atoms per unit cell with lattice parameters $a_0 = 3.784$ Å and $c_0 = 9.514$ Å.[37] The titanium atom is coordinated with six oxygens at two different Ti-O distances: four at 1.934 Å and two others at 1.980 Å. The atomic cluster, described in Table

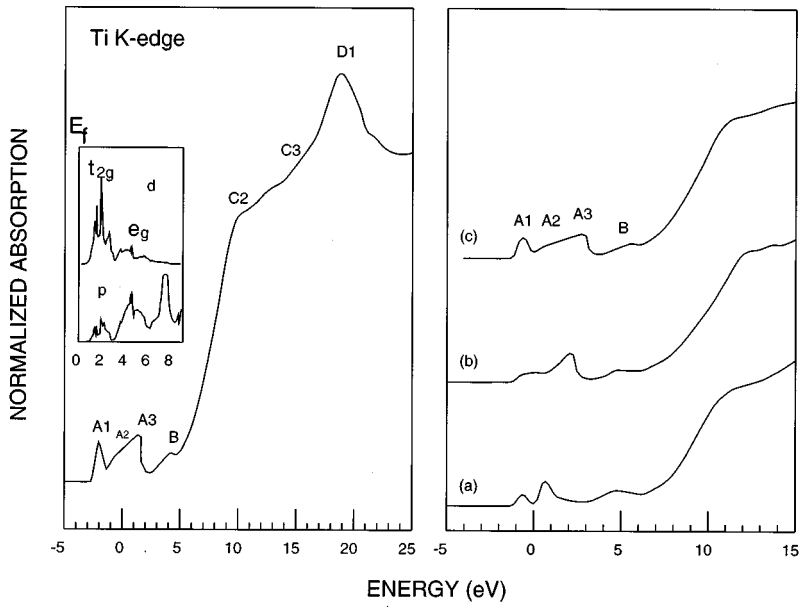

FIG. 8. Theoretical computations of XANES spectra at Ti K edge for anatase. Left panel: 91-atom cluster contribution. The inset gives the theoretical TB-LMTO Ti p-DOS (lower curve) multiplied by 35, d-DOS (upper curve). Right panel: (a) Simplified cluster calculation with the same size as used in left panel (91-atom cluster), but by taking into account solely four Ti1 at 3.039 Å (see Table I) (i.e., suppressing four Ti2 at 3.784 Å from the 91-atom cluster). (b) The same as (a) but taking into account the contributions of four Ti2 at 3.784 Å (suppressing four Ti1 at 3.039 Å from the second shell in the 91-atom cluster). (c) The same as the curve in left panel in energy region -5–15 eV.

I up to 4.0 Å, has D_{2d} point group symmetry. In the left panel of Fig. 8 we present the computed Ti K-edge XANES spectrum relative to a 91-atom cluster which has reached size convergence. It can be seen that all experimental features are reasonably well reproduced as illustrated in Table II: three prepeaks $A1$, $A2$, and $A3$, corresponding to transitions to $3d$-$4p$ hybridized states, structure B, which has basically the same origin as peak B in rutile, assigned to transition to a_1 type of orbitals, features $C2$ and $C3$ again related to $4p$ levels of b_3 and e symmetry appropriate for anatase and peak D attributed to higher-lying p orbitals. The inset contains the DOS just above the Fermi level E_f as shown in Fig. 7. Reasonable agreement is achieved with MS cluster calculation: peaks $A1$–$A3$ arise dominantly from the hybridization of $3d$-$4p$ orbitals, and feature B has mainly p character. It is worthwhile noticing that there are three preedge peaks of the A type at a variance from the rutile case. In order to understand the origin of this extra peak, in the right panel of Fig. 8 we present two different calculations which take into account separately the contributions from the two second neighboring Ti subshells (see Table I). Clearly the four Ti at 3.039 Å contribute to features $A1$ and $A2$, while the four Ti at 3.784 Å contribute to $A1$ and $A3$. Their sum is almost equal to the 91 atom cluster calculation as shown by curve (c). At variance with the rutile case, here there are two e_g peaks, $A2$ and $A3$, reflecting not only crystal field effects but also a different degree of hybridization with the central Ti $4p$ orbitals due to the different distance of the two Ti shells. As pointed out in Ref. 12 this distance-dependent hybridization mechanism can also be invoked to explain why the preedge intensity in the case of anatase is lower than in rutile. In fact the amplitude for the p character of the central atom wave function decreases for increasing values of the Ti-Ti distances, which are indeed expanded in anatase compared to rutile. Notice also that in this case transitions to $3d$ on the central Ti atoms are dipole allowed. They are taken into account by the MS calculations but do not seem to contribute much to the preedge intensity.

C. Oxygen K edge for rutile and anatase

In electron-energy-loss spectra one measures dipolar transitions similar to those probed by XAS, provided the signal is collected at small scattering angles off the incident electron beam. The interpretation of ELNES follows therefore similar lines as that of XANES.[38] In Fig. 9 we present MS calculations of the O K-edge spectra in the case of rutile, using different cluster sizes (4, 15, 28, 43, and 61 atoms). The atomic cluster around the central O up to 4 Å is shown in Table III. For a four atom cluster, consisting of an O central atom plus the first coordination shell of three Ti atoms, one already obtains a prepeak A, which is however not split into two components. This feature reflects transitions to

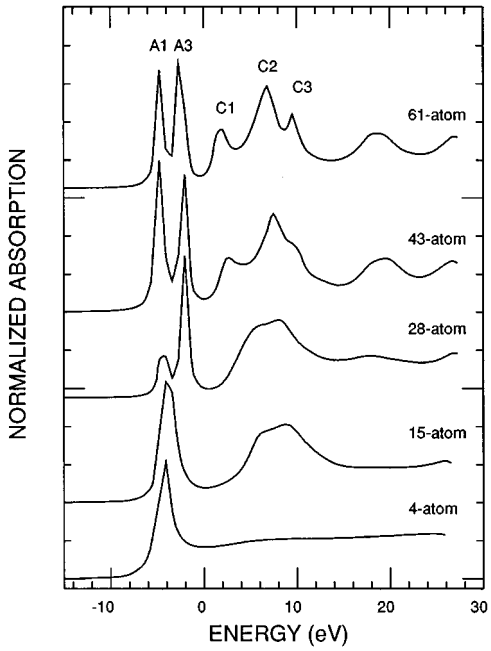

FIG. 9. MS calculations of the oxygen K-edge XANES spectra in rutile as a function of cluster size.

TABLE III. Coordinates and interatomic distances (in Å) for the atomic clusters around photoabsorber O up to 4 Å. Only symmetrically nonequivalent atoms are included. The point group is C_{2v} for both rutile and anatase. The z axis is along the c axis of the compounds.

	Atom	x	y	z	Dist.	Atom	x	y	z	Dist.
			TiO_2-rutile					TiO_2-anatase		
1	O ×1	0.0000	0.0000	0.0000	0.0000	O ×1	0.0000	0.0000	0.0000	0.0000
2	Ti×2	0.0000	1.4795	1.2682	1.9487	Ti×2	0.0000	1.8920	0.3986	1.9335
3	Ti×1	0.0000	0.0000	−1.9803	1.9803	Ti×1	0.0000	0.0000	−1.9799	1.9799
4	O ×1	0.0000	0.0000	2.5364	2.5364	O ×2	0.0000	1.8920	−1.5812	2.4658
5	O ×4	1.2682	1.4795	−1.9803	2.7783	O ×4	1.8920	1.8920	0.7973	2.7919
6	O ×4	1.9803	1.4795	1.2682	2.7783	O ×2	1.8920	0.0000	−2.3785	3.0392
7	O ×2	0.0000	2.9590	0.0000	2.9590	O ×2	0.0000	1.8920	2.3785	3.0392
8	O ×2	3.2484	0.0000	−0.7121	3.3255	O ×2	1.8920	0.0000	3.1758	3.6967
9	Ti×2	3.2484	0.0000	1.2682	3.4872	O ×2	3.7840	0.0000	0.0000	3.7840
10	Ti×2	0.0000	2.9590	−1.9803	3.5605	O ×2	0.0000	3.7840	0.0000	3.7840
11	O×2	0.0000	2.9590	2.5364	3.8973	Ti×4	1.8920	1.8920	2.7771	3.8564
12	O×1	0.0000	0.0000	−3.9605	3.9605	O ×1	0.0000	0.0000	−3.9597	3.9597

the O $2p$ states hybridized with the Ti $3d$ states localized at the Ti sites.[39] Experimentally this peak splits into two components $A1$ and $A3$. de Groot *et al.*[39] have interpreted these two peaks as due to dipole transitions to band states of t_{2g}-e_g symmetry separated by the ''ligand-field splitting.'' The splitting is in fact reproduced by our MS approach when using larger clusters as shown by the 28-, 43-, and 61-atom cluster calculations, respectively. In order to better illustrate its origin, we present in Fig. 10 a simplified 20-atom cluster calculation (see Table III), which contains the central O, its nearest three Ti atoms, and the outer neighboring 16 oxygen atoms that provide exactly an octahedral environment for these three Ti. The doublet labeled $A1$ and $A3$ is very well defined. This is further evidence, once again, that the splitting of the preedge peak in anion spectra is due to the hybridization of the oxygen $2p$ orbitals with the metal $3d$ orbitals electrostatically split by the local octahedral crystal field, as found in other $3d$ transition-metal oxides.[40–42]

We present in Fig. 11 a comparison between the fully relaxed final state (by $Z+1$ approximation[24]) and the ground-state potentials calculations. There is no significant difference between them apart from a slight rigid energy shift of about 0.5 eV of the entire spectrum. This result indicates that the preedge peaks $A1$ and $A3$ cannot be ascribed to the formation of core-exciton states split down from the conduction band.

The features $C1$, $C2$, and $C3$ can be attributed to oxygen $2p$ states hybridized with titanium $4s$ and $4p$ states[39,43] of the right symmetry. Notice that the point group symmetry is

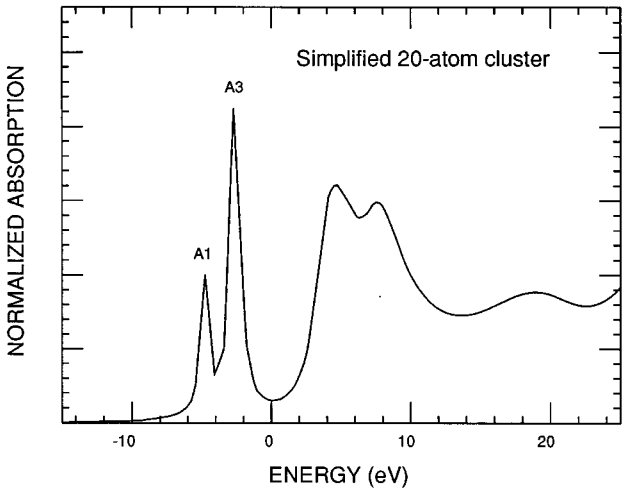

FIG. 10. MS calculations of O *K*-edge XANES spectra in rutile by using a simplified 20-atom cluster: central oxygen plus the nearest three Ti and 16 oxygens as shown in Table III (not taking into account the contributions of two Ti at about 3.487 Å and 3.560 Å, respectively).

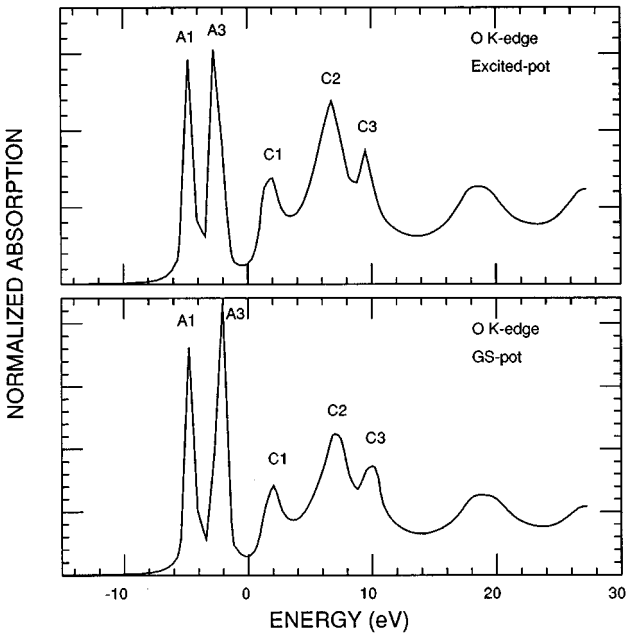

FIG. 11. Comparison between MS calculations of the oxygen *K*-edge XANES spectra in rutile by using different potentials. Upper panel: excited final state potential; lower panel: ground state (GS) potential.

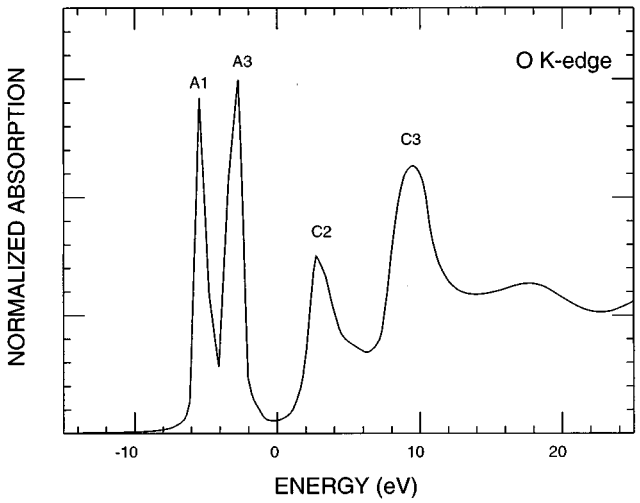

FIG. 12. MS calculations of the oxygen K-edge XANES spectra in anatase by using 47-atom cluster.

C_{2v}. From the MS point of view their origin can be monitored by looking at the various cluster calculations of Fig. 9. They are indeed the counterpart of the same features as seen from the Ti K edge and for this reason have been labeled in the same way. This fact allows us to obtain a confirmation of the spectral assignments of the various features in the preedge region of the Ti K-edge spectra. As indeed seen from Table II, the experimental energy distances between the A and the C peaks in the O K-edge spectra coincide with those of the corresponding features at the Ti K edge. In particular this is true for the first $A1$ peak. Therefore the spectral assignment of the A peaks in the spectra of both edges must be the same. Since there is no doubt on the assignment of peak $A1$ at the O K edge as being due to a t_{2g} bandlike state, we conclude that this is also true at the Ti K edge. Notice that peak B seems to be missing in the O K-edge spectra, probably because it falls into a minimum between the $A3$ and $C1$ features.

Summarizing, not only the energy positions but also the relative amplitudes of the features $A1$, $A3$, $C1$, $C2$, and $C3$ at the O K edge are in good agreement with the experimental data. The extensive spread in energy of the oxygen $2p$ states is an indication of significant covalency in these oxides.

In Fig. 12, we show a 47-atom cluster calculation at O K edge in anatase. In this case the symmetry point group is also C_{2v}. Overall the theoretical spectrum is in good agreement with experimental data for all peak positions and relative intensities. The peaks $A1$ and $A3$ have basically the same origin as those in rutile. Again peaks $C2$ and $C3$ arise from transitions to oxygen $2p$ hybridized with Ti $4p$ states of respective local symmetry b_3 and e in their octahedral environment. The $C3$ distance from the A features is in good agreement with the same distances in the Ti K edge of anatase. However the distance $A1$-$C2$ seems to present a problem here, being 2 eV wider than in the corresponding O K-edge spectrum. We ascribe this discrepancy to the spread in outer Ti shell distances around the central Ti atom in anatase.

IV. CONCLUSIONS

We have carried out a detailed theoretical investigation of Ti and O K-edges XANES/ELNES spectra for both rutile and anatase. We have obtained good agreement with experimental data using one-electron full MS calculations. Since our one-electron MS theory includes only the dipole-allowed transitions, the good agreement between experimental data and theoretical calculations indicates that all the peaks appearing in the spectra of Ti and O K edges correspond to transitions to states which have at least a significant amount of p symmetry. In fact, for the Ti K-edge absorption, symmetry considerations show that the p orbitals of the central Ti atom can mix with d orbitals of the higher-neighboring Ti octahedra. Even in the centrosymmetric systems such combinations can give rise to u character.[12,44,45] The first nearest-neighbor geometrical arrangement around a central atom in both rutile and anatase is quite similar as shown in Table I and Table III. Then the differences in the Ti and O K-edge XANES/ELNES spectra should arise from the outer-lying atomic shells, indicating that the long-range effects play an important role in determining the near-edge structures.[46,47] We are able to model these differences reasonably well at the Ti K and O K edges using increasing atomic clusters up to convergence and $X-\alpha$ exchange-correlation potential.

All the transition features in the preedge region of Ti K-edge and O K-edge XANES/ELNES spectra are not difficult to explain by a mixing of $4p$ orbital of the absorbing atom with $3d$ orbitals of higher-neighboring Ti octahedra or oxygen $2p$ states with the nearest Ti octahedral orbitals, respectively. In particular, we tend to assign the prepeaks $A1$ and $A3$ at the Ti K edge to transitions to t_{2g} and e_g bandlike states based on the comparison between TB-LMTO DOS and cluster MS calculations which take into account the different contributions from Ti subshells. Comparison with the corresponding O K-edge spectra further confirms these assignments. The results for anatase both at the Ti and O K edge are interpreted along similar lines and reinforce the interpretation given for rutile. Finally feature B has mainly p character and could be assigned to transitions to $4p$ states hybridized with a_g or a_1 states on neighboring sites, for rutile and anatase, respectively, on the basis of the comparison with TB-LMTO DOS calculations.

Summarizing, our conclusions are not very much different from those reached in Refs. 7 and 12, although we think we have justified more in depth the spectral assignments of the various absorption features. Moreover our calculations are closer to the experimental spectra. We have also argued against the assignment made in Ref. 16 of the first transition feature $A1$ in rutile as due to a pure quadrupole transition, on the basis not only of the comparison with the O K edge and anatase spectra but also of some drawbacks in the particular Hubbard model used for TiO_2.

ACKNOWLEDGMENTS

We thank Professor O. Jepsen and Dr. F. Boucher for constructive discussions. This work was supported by a Human Capital and Mobility EC grant (Z.Y.W.).

[1] J.M. Heintz, M. Drillon, R. Kuentzler, Y. Dossmann, J.P. Kappler, O. Durmeyer, and F. Gautier, Z. Phys. B **76**, 303 (1989).
[2] A.F. Carley, P.R. Chalker, J.C. Riviere, and M.W. Roberts, J. Chem. Soc. Faraday Trans. **83**, 351 (1987).
[3] H. Kung, in *Studies in Surface and Catalysis*, Transition Metal Oxides, Vol. 45, edited by B. Delmon and J.T. Yates (Elsevier, Amsterdam, 1989), Chaps. 10 and 14.
[4] G.A. Waychunas, J. Phys. (Paris) Colloq. **C8**, 841 (1986); Am. Mineral. **72**, 89 (1987).
[5] L. Soriano, M. Abbate, J.C. Fuggle, M.A. Jimenez, J.M. Sanz, C. Mythen, and H.A. Padmore, Solid State Commun. **87**, 699 (1993).
[6] F.M.F. de Groot, M.O. Figueiredo, M.J. Basto, M. Abbate, H. Petersen, and J.C. Fuggle, Phys. Chem. Miner. **19**, 140 (1992).
[7] R. Brydson, H. Sauer, W. Engel, J.M. Thomas, E. Zeitler, N. Kosugi, and H. Kuroda, J. Phys. Condens. Matter **1**, 797 (1989).
[8] R. Brydson, B.J. Williams, W. Engel, H. Sauer, E. Zeitler, and J.M. Thomas, Solid State Commun. **64**, 609 (1987).
[9] L.A. Grunes, R.D. Leapman, C.N. Wilker, R. Hoffmann, and A.B. Kunz, Phys. Rev. B **25**, 7157 (1982).
[10] L.A. Grunes, Phys. Rev. B **27**, 2111 (1983).
[11] B. Poumellec, J.F. Marucco, and B. Touzelin, Phys. Rev. B **35**, 2284 (1987); B. Poumellec, P.J. Durham, and G.Y. Guo, J. Phys. Condens. Matter **3**, 8195 (1991).
[12] M.F. Ruiz-Lopez and A. Munoz-Paez, J. Phys. Condens. Matter **3**, 8981 (1991).
[13] G. Van der Laan, C.S. Mythen, and H.A. Padmore, Europhys. Lett. **11**, 67 (1990).
[14] C. Cartier and M. Verdaguer, J. Chem. Phys. **86**, 1607 (1989).
[15] M.A. Khan, A. Kotani, and J.C. Parlebas, J. Phys. Condens. Matter **3**, 1763 (1991).
[16] T. Uozumi, K. Okada, A. Kotani, O. Durmeyer, J.P. Kappler, E. Beaurepaire, and J.C. Parlebas, Europhys. Lett. **18**, 85 (1992).
[17] C. Brouder, J.P. Kappler, and E. Beaurepaire, *2nd European Conference on Progress in X-ray Synchrotron Radiation Research*, edited by A. Balerna, E. Bernieri, and S. Mobilio (SIF, Bologna, 1990), Vol. 25, p. 19.
[18] B. Poumellec, R. Cortes, G. Tourillon, and J. Berthon, *2nd European Conference on Progress in X-ray Synchrotron Radiation Research* (Ref. 17), p. 23.
[19] P.A. Lee and J.B. Pendry, Phys. Rev. B **11**, 2795 (1975).
[20] C.R. Natoli, D.K. Misemer, S. Doniach, and F.W. Kutzler, Phys. Rev. A **22**, 1104 (1980); C.R. Natoli, and M. Benfatto, J. Phys. (Paris) Colloq. **47**, C8-11 (1986); C.R. Natoli, M. Benfatto, C. Brouder, M.Z. Ruiz Lopez, and D.L. Foulis, Phys. Rev. B **42**, 1944 (1990); T.A. Tyson, K.O. Hodgson, C.R. Natoli, and M. Benfatto, *ibid.* **46**, 5997 (1992).
[21] P.J. Durham, J.B. Pendry, and C.H. Hodges, Comput. Phys. Commun. **25**, 193 (1982).
[22] A. Bianconi, in *X-ray Absorption: Principles, Applications, Techniques of EXAFS, SEXAFS, XANES*, edited by R. Prinz and D. Koningsberger (Wiley, New York, 1988).
[23] P.J. Durham, in *X-ray Absorption: Principles, Applications, Techniques of EXAFS, SEXAFS, XANES* (Ref. 22).
[24] P.A. Lee and G. Beni, Phys. Rev. B **15**, 2862 (1977).
[25] C.R. Natoli (unpublished).
[26] Z.Y. Wu, M. Benfatto, and C.R. Natoli, Phys. Rev. B **45**, 531 (1992); Solid State Commun. **87**, 475 (1993); Z.Y. Wu, F. Seifert, B. Poe, and T. Sharp, J. Phys. Condens. Matter **8**, 3323 (1996); Z.Y. Wu, A. Mottana, A. Marcelli, C.R. Natoli, and E. Paris, Phys. Chem. Miner. **23**, 193 (1996); Z.Y. Wu, A. Marcelli, A. Mottana, G. Giuli, E. Paris, and F. Seifert, Phys. Rev. B **54**, 2976 (1996).
[27] L. Mattheiss, Phys. Rev. A **134**, 970 (1964).
[28] E. Clementi and C. Roetti, At. Data Nucl. Data Tables, **14**, 177 (1974).
[29] D.R. Penn, Phys. Rev. B **35**, 482 (1987).
[30] J.G. Norman, Mol. Phys. **81,** 1191 (1974).
[31] (a) O.K. Andersen, Phys. Rev. B **12**, 3060 (1975); O.K. Andersen and O. Jepsen, Phys. Rev. Lett. **53**, 2571 (1984); O.K. Andersen, O. Jepsen, and M. Sob, in *Electronic Band Structure and Its Applications*, edited by M. Yussouff (Springer-Verlag, Berlin, 1986); (b) O. Jepsen and O.K. Andersen, Z. Phys. B **97**, 35 (1995); (c) W.R. Lambrecht and O.K. Andersen, Phys. Rev. B **34**, 2439 (1986); (d) P.E. Blöchl, O. Jepsen, and O.K. Andersen, *ibid.* **49**, 16 223 (1994).
[32] (a) O.K. Andersen, H.L. Skriver, H. Nohl, and B. Johansson, Pure Appl. Chem. **52**, 93 (1979); (b) O.K. Andersen, O. Jepsen, A.I. Liechtenstein, and I.I. Mazin, Phys. Rev. B **49**, 4145 (1994).
[33] H.L. Skriver, in *The LMTO Method*, edited by J.C. Fuggle and J.E. Inglesfield, Unoccupied Electronis States, Topics in Applied Physics Vol. 69 (Springer-Verlag, Berlin, 1992), Chaps. 2, 3, and 5.
[34] Z.Y. Wu, G. Ouvrard, S. Lemaux, P. Moreau, P. Gressier, F. Lemoigno, and J. Rouxel, Phys. Rev. Lett. **77**, 2101 (1996); Z.Y. Wu, F. Lemoigno, P. Gressier, G. Ouvrard, P. Moreau, J. Rouxel, and C.R. Natoli, Phys. Rev. B **54**, 11 009 (1996).
[35] V.I. Anisimov, J. Zaanen, and O.K. Andersen, Phys. Rev. B **44**, 943 (1991).
[36] S.C. Abrahams and J.L. Bernstein, J. Chem. Phys. **55**, 3206 (1971).
[37] C.J. Howard, T.M. Sabine, and F. Dickson, Acta Crystallogr. Sec. B **47**, 462 (1991).
[38] R.F. Egerton, *Electron Energy Loss Spectroscopy in the Electron Microscope* (Plenum, New York, 1986).
[39] F.M.F. de Groot, M. Grioni, J.C. Fuggle, J. Ghijsen, G.A. Sawatzky, and H. Petersen, Phys. Rev. B **40**, 5715 (1989).
[40] Z.Y. Wu, S. Gota, F. Jollet, M. Pollak, M. Gautier-Soyer, and C.R. Natoli, Phys. Rev. B **55**, 2570 (1997).
[41] H. Kurata, E. Lefèvre, C. Colliex, and R. Brydson, Phys. Rev. B **47**, 13 763 (1993).
[42] C. Colliex, T. Manoubi, and C. Ortiz, Phys. Rev. B **44**, 11 402 (1991).
[43] J. Ghijsen, L. H. Tjeng, J. Van Elp, H. Eskes, J. Westerink, G. A. Sawatzky, and M. T. Czyzyk, Phys. Rev. B **38**, 11 322 (1988).
[44] C.J. Ballhausen, *An Introduction to Ligand Field Theory* (McGraw-Hill, New York, 1962).
[45] S.F.A. Kettle, *Symmetry and Structure* (Wiley, New York, 1985).
[46] S.H. Chou, J.J. Rehr, E.A. Stern, and E.R. Davidson, Phys. Rev. B **35**, 264 (1987).
[47] A. Di Cicco, N.V. Pavel, A. Bianconi, M. Benfatto, and C.R. Natoli, J. Phys. (Paris) Colloq. **47**, C8-71 (1986); L.A. Bugaev, I.I. Gegusin, A.A. Novakovich, and R.V. Vendrinskii, *ibid.* **47**, C8-101 (1986); P. Sainctavit, J. Petiau, M. Benfatto, and C.R. Natoli, Physica B **158**, 347 (1989).